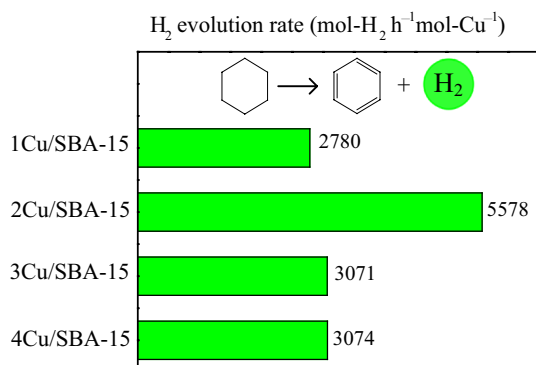CrossMark

High Selectivity of Cyclohexane Dehydrogenation for H_2 Evolution Over Cu/SBA-15 Catalyst

Zhijun Xia[1] · Huayan Liu[1] · Hanfeng Lu[1] · Zekai Zhang[1] · Yinfei Chen[1]

Abstract The effects of metal particle size on catalytic activities of Cu/SBA-15 with different Cu content were investigated for high selectivity of cyclohexane dehydrogenation. Overall, the smaller Cu nanoparticles exhibit higher hydrogen evolution rate or lower active energy barrier. But, even when the smaller CuO nanoparticles have formed on the catalyst with lower Cu content during the calcination, they would be more prone to sinter after reduction. An appropriate Cu content could lead to form amounts of stable and small Cu nanoparticles after high-temperature treatment with the space limitation by ordered channels of SBA-15.

Graphical Abstract

H_2 evolution rate (mol-H_2 h^{-1}mol-Cu^{-1})

1Cu/SBA-15 2780
2Cu/SBA-15 5578
3Cu/SBA-15 3071
4Cu/SBA-15 3074

✉ Yinfei Chen
chfy@zjut.edu.cn

Zhijun Xia
xiazj919@163.com

1   Institute of Catalytic Reaction Engineering,
    College of Chemical Engineering, Zhejiang
    University of Technology, Hangzhou 310014,
    People's Republic of China

1 Introduction

Hydrogen has been regarded as a clean fuel. But its storage remains a problem [1–3]. The organic hydride method for hydrogen storage, transportation and supply has been potential industrial candidates, due to its simple, security, efficiency and CO_x free hydrogen [3–6]. In particular, cyclohexane holds high hydrogen content about 56.0 g L^{-1} (volume capacity) and 7.1% (mass percent). Although the endothermic energy requirement for cyclohexane dehydrogenation is 68.8 kJ mol^{-1} of H_2, this is much lower than energy 248 kJ mol^{-1} of H_2 oxidation reaction. Furthermore, the application of hydrogen can facilitate the saving of a great amount of CO_2 emissions by replacing gasoline and diesel used in disperse or mobile facilities with H_2 [6]. Moreover, the hydrogenation process from the dehydrogenation product benzene to cyclohexane is mature, and provides an additional advantage for the reversible catalytic hydrogenation–dehydrogenation reactions. Thus, the intensive research efforts have been done in cyclohexane dehydrogenation for hydrogen delivered [7–11].

Additionally, many attempts have been made to replace precious Pt-based catalysts which have good performance for the dehydrogenation reaction of cyclohexane [10, 11], in order to reduce the cost of hydrogen storage [7–9]. Including the earlier research of Sinfelt et al. [12], Ni–Cu bimetallic catalysts have emerged good catalytic performance for the dehydrogenation reaction of cyclohexane, and the Cu addition into Ni-based catalysts improves the selectivity to benzene. In fact, the monometallic Cu-based catalyst presents close to 100% selectivity to benzene even up to high

🖄 Springer

temperature 375 °C, although its conversion is less than that of Ni-based catalyst [8]. Furthermore, because of that Cu has lower melting point and Tammann temperature than that of Ni, Cu is more prone to be migrated to the surface of metallic particles [13]. Therefore, Cu plays important roles on the selectivity of this reaction. However, a special study on Cu-based catalysts for dehydrogenation reaction of cyclohexane has not been developed yet.

The monometallic Cu-based catalysts have been used frequently, due to its high activity and selectivity on hydrogenation [14–16], dehydrogenation [17, 18] and water–gas reforming reaction [19, 20]. The catalytic activity of Cu-based catalyst would be dramatically improved as the particle size of Cu nanoparticles decreased [21]. However, the preparation of highly dispersed Cu nanoparticles is difficult, due to sintering easily for CuO or Cu nanoparticles during thermal treatments [19]. Recently, SBA-15 with regular channels and high surface area has been used widely as catalytic supporters to load Cu nanoparticles [14, 19, 22–24]. The sintering would be suppressed by the space limitation of the ordered channels of SBA-15.

In this work, in order to investigated the catalytic performance of Cu-based catalysts, mesoporous SBA-15 was employed to support and disperse metal Cu with different content. Thereafter, a series of characterizations were performed to reveal properties of catalysts and the relationship between cyclohexane dehydrogenation and Cu-based catalysts.

2 Experimental

2.1 Catalyst Preparation

The Cu/SBA-15 catalysts were prepared by impregnation, according to the recipe reported in document [25]. Briefly, 0.30, 0.60, 0.90 or 1.20 mmol $Cu(NO_3)_2 \cdot 3H_2O$ (Sinopharm Chemical Reagent Co., 99% purity) was dissolved into solvent mixed with 5.00 g hexane (Sinopharm Chemical Reagent Co., 99.5% purity) and 5.00 g alcohol (Sinopharm Chemical Reagent Co., 99.8% purity). Then, 1.00 g mesoporous SBA-15 (JCNANO, 685.4 $m^2\ g^{-1}$) was added into the impregnation solution. After drying at room temperature for 24 h and 60 °C for 24 h, the samples were calcined at 550 °C for 4 h. Finally, the samples were obtained and denoted as 1Cu/SBA-15, 2Cu/SBA-15, 3Cu/SBA-15 and 4Cu/SBA-15, respectively.

2.2 Catalyst Characterization

Nitrogen adsorption–desorption measurements were performed at −196 °C with a Micromeritics 3Flex Surface Characterization Analyzer. Prior to measurement, the

samples were degassed at 280 °C for 5 h. Specific surface area, porosity and pore size distribution of all the samples were calculated using BET (Brunaure, Emmett and Teller) and BJH (Barrett, Joyner and Halenda).

Powder X-ray diffraction (XRD) patterns were collected in the 2θ range of 10°–80° on a PANalytical X'Pert PRO diffractometer with Cu Kα radiation ($\lambda = 0.154$ nm).

Hydrogen temperature-programmed reduction (H_2-TPR) experiments were carried out on a FineSORB-3010 apparatus. Firstly, 50 mg of sample was loaded into a U-shape quartz reactor and pretreated with Ar at 200 °C for 1 h. Then, after cooling to 50 °C under Ar, the gas flow was switched to 5% H_2 in Ar (30 mL min^{-1}), and the sample was heated to 800 °C at 10 °C min^{-1}. The amount of hydrogen consumption was recorded with a thermal conductivity detector.

Diffuse reflectance UV–Visible (DR UV–Vis) spectra were recorded on a UV-2600 (Shimadzu) spectrophotometer, operating at room temperature in the wave length range of 200–800 nm.

Raman data was collected with an inVia Raman microscope (Renishaw) with 180 s in the wave-number range of 100–1200 cm^{-1}.

High-resolution transmission electron microscopy (HRTEM) was performed with a Philips-FEI Tecnai G2 F30 S-Twin instrument operated at 300 kv.

2.3 Catalytic Reaction

Cyclohexane dehydrogenation reaction was carried out in a fixed-bed microreactor (internal diameter 5 mm) with a feed composition of C_6H_{12}: $H_2 = 1:25$ (molar ratio). Typically, after the sample reduced at 450 °C with a H_2 flow (30 mL min^{-1}) for 4 h and cooled to reaction temperature, cyclohexane was introduced to the reactor by bubbling H_2 at 0 °C ice water bath, and the feed gas with a total flow (30 mL min^{-1}) was passed over 150 mg of sample (40–60 mesh), resulting in a gas hourly space velocity (GHSV) 12,000 mL $g^{-1}\ h^{-1}$. The products were analyzed on-line by peak area normalization method with an Agilent GC-7890A, equipped with FID detector and a HP-INNOWax capillary column. The conversion of cyclohexane, the selectivity to benzene (or H_2) and the evolution rate of H_2 were calculated as:

$$\text{Conversion of } C_6H_{12} = \frac{\text{Moles of } C_6H_{12}\ \text{reacted}}{\text{Moles of } C_6H_6\ \text{in feed}} \times 100\%$$

$$\text{Selectivity of } C_6H_6 = \frac{\text{Moles of } C_6H_6\ \text{in product}}{\text{Moles of } C_6H_6\ \text{reacted}} \times 100\%$$

$$H_2\ \text{evolution rate} = \frac{3 \times \text{Moles of } C_6H_6\ \text{in product}}{\text{Moles of Cu in catalyst} \times \text{Reaction time}}$$

3 Results and Discussion

3.1 Catalytic Activity

As shown in Fig. 1a, the conversion of cyclohexane on Cu/SBA-15 catalysts in this work is no more than 25%, while no any other product was detected which means that the selectivity toward benzene is 100%, even up to 400 °C. However, more interesting is that the hydrogen evolution rate at 350 °C for per mole Cu atoms of 2Cu/SBA-15 is about double of that in other catalysts. The small Cu particles provides a higher reaction rate than that of bulk Cu [19], indicating its lower active energy barrier. The apparent activation energy (*Ea*) was calculated from the slope of Arrhenius plots of each catalyst (Fig. 2) [17, 26], and used to evaluate catalytic activity. It is obvious that the *Ea* (74.7 J mol^{-1} K^{-1}) of 2Cu/SBA-15 in the temperature range of 300–400 °C is lower than that (80–82 J mol^{-1} K^{-1}) of other catalysts. Therefore, we deduce that amounts of small Cu particles exit in the 2Cu/SBA-15 which result to higher hydrogen evolution rate, compared with other catalysts.

3.2 Characterization of Catalysts

3.2.1 Textural Properties

Nitrogen adsorption–desorption measurements were used to evaluate the textural properties of SBA-15 and calcined samples (Fig. 3; Table 1). All the Cu/SBA-15 catalysts present the same Type-IV isotherm and a H1 hysteresis loop to the SBA-15. This means the mesoporous nature for the catalysts after calcination is maintained. The BET surface area as well as pore volume decrease with the loading of
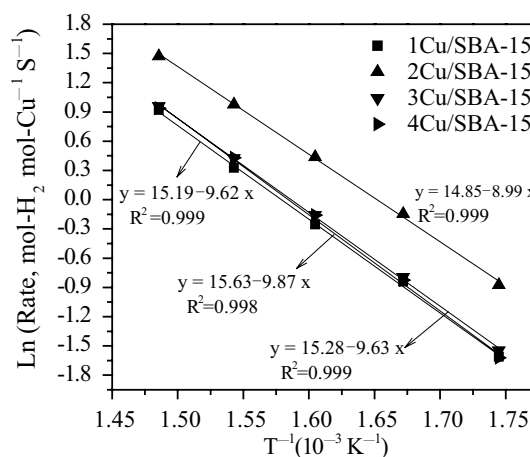

Fig. 2 Arrhenius plots of Cu/SBA-15 catalysts for cyclohexane dehydrogenation

Cu, while the average pore size increases. However, the micropores diminish, the pores about 3 nm appear, and the pores in the size range of 5–7 nm decrease in the Cu/SBA-15, compared with blank SBA-15. These imply that the CuO precursor enters into the mesoporous channels, and blocks partially the entrance, in according with the previous report [14].

3.2.2 Surface Analysis

Figure 4 shows the XRD patterns of calcined and spent catalysts under ambient condition. The distinct peak of CuO (PDF #48-1548) is observed for all catalysts after calcination (Fig. 4a). And the mean particle size (Table 1) calculated using Scherrer equation reduces as the Cu content
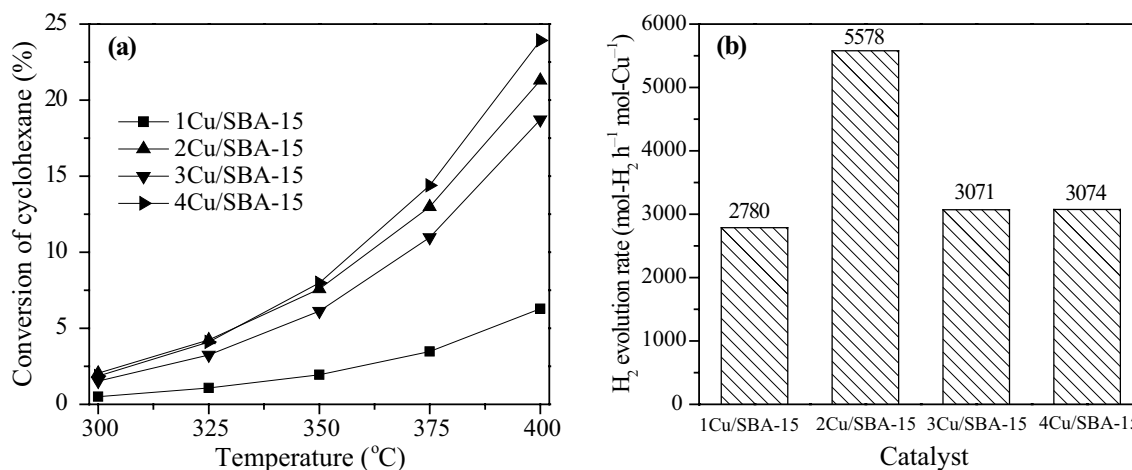

Fig. 1 Catalytic activity of Cu/SBA-15 catalysts (150 mg, total 101 kPa, C$_6$H$_{12}$: H$_2$ = 1:25, GHSV = 12,000 h^{-1}). **a** Conversion of cyclohexane and **b** H$_2$ evolution rate at 350 °C
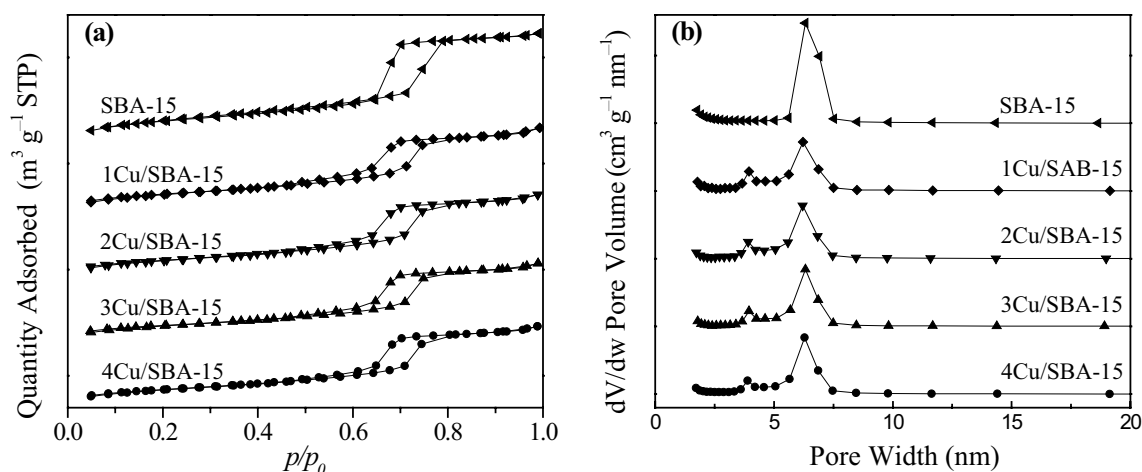
Fig. 3 N_2 adsorption–desorption isotherms (**a**) and pore size distribution (**b**) of SBA-15 and the calcined Cu/SBA-15 catalysts

Table 1 The physicochemical properties of Cu/SBA-15 catalysts

Catalyst	Cu loading[a] (wt%)	S_{BET} (m^2 g^{-1})	Pore volume (cm^3 g^{-1})	Pore size (nm)	Crystal size[b] (nm) CuO	Cu
SBA-15	0	685.4	0.95	5.54	–	–
1Cu/SBA-15	1.88	517.0	0.72	5.61	20.1	33.7
2Cu/SBA-15	3.70	483.2	0.70	5.81	26.7	42.2
3Cu/SBA-15	5.45	458.8	0.66	5.80	28.0	39.6
4Cu/SBA-15	7.13	451.0	0.67	5.90	32.5	33.9

[a]Cu/(Cu + SBA-15) as determined according to the preparation of catalyst

[b]Calculated using Scherrer equation from XRD patterns

decreased, consistent with the result reported by Vargas-Hernandez et al. [14]. Furthermore, it is larger than the average size of pores inside of catalysts, indicating the sintering of CuO particles on the exterior surface and in the channels.

For the spent catalysts after reaction for total 5 h (per hour at each reaction temperature), their XRD patterns show three sharp peaks at $2\theta = 43.4°$, $50.5°$ and $74.3°$, attributed to Cu (PDF #65-9743). The intensity of the peaks becomes gradually weaker with the decrease of Cu content, as the same trend with that of the calcined catalysts. However, the mean particle size of metal Cu presents an increase trend in contrast, except for 1Cu/SBA-15. This is mainly because of that the strong intensity depends on not only crystallite size and crystallinity, but also Cu content on the supporter. Moreover, the smaller Cu crystal particles are more liable to gather and lead to the formation of large Cu particles [14]. In addition, the small Cu particles in the pores of SBA-15 could be also aggregation, but their size is limited by the ordered channels.

Figure 5 shows the TEM images of the spent Cu/SBA-15 samples. The particles on the exterior surface of all catalysts seem like lying on the face or being inside the pores, similar with the previous reports [13, 19]. And no obvious particles were observed outside the pores. These would imply that the particles presented on the exterior surface come from the internal surface of the pores, and block the pore mouth. Nonetheless, the ordered channels of SBA-15 were kept well, agreed with the result of N_2 adsorption–desorption measurements.

In the order to further investigate the surface species, UV–vis DRS spectra (Fig. 6) and Raman spectra (Fig. 7) of the spent catalysts were performed. In Fig. 6, the large band centered at 250 nm in the range of 200–300 nm is attributed to SiO_2 [27]. The shoulder peak at 370 nm is ascribed to charge transfer bands of (O–Cu–O) [28], indicating the existence of highly dispersive Cu species which was oxidized easily and not observed in the XRD patterns. The weak peak at 575 nm is attributed to Cu_n plasmon resonance [28]. The intensity of these signals declines gradually with the decease of Cu content. In Fig. 7, the Raman
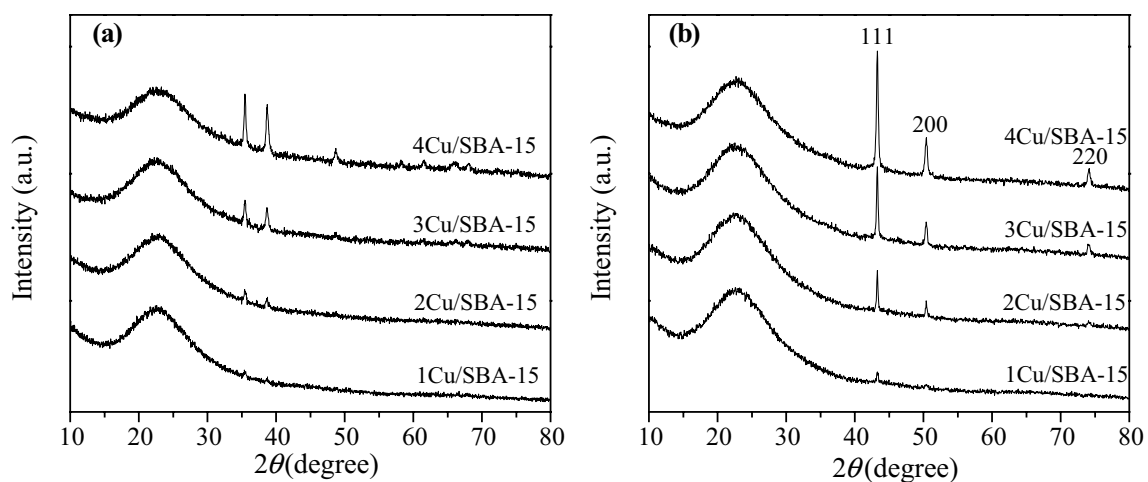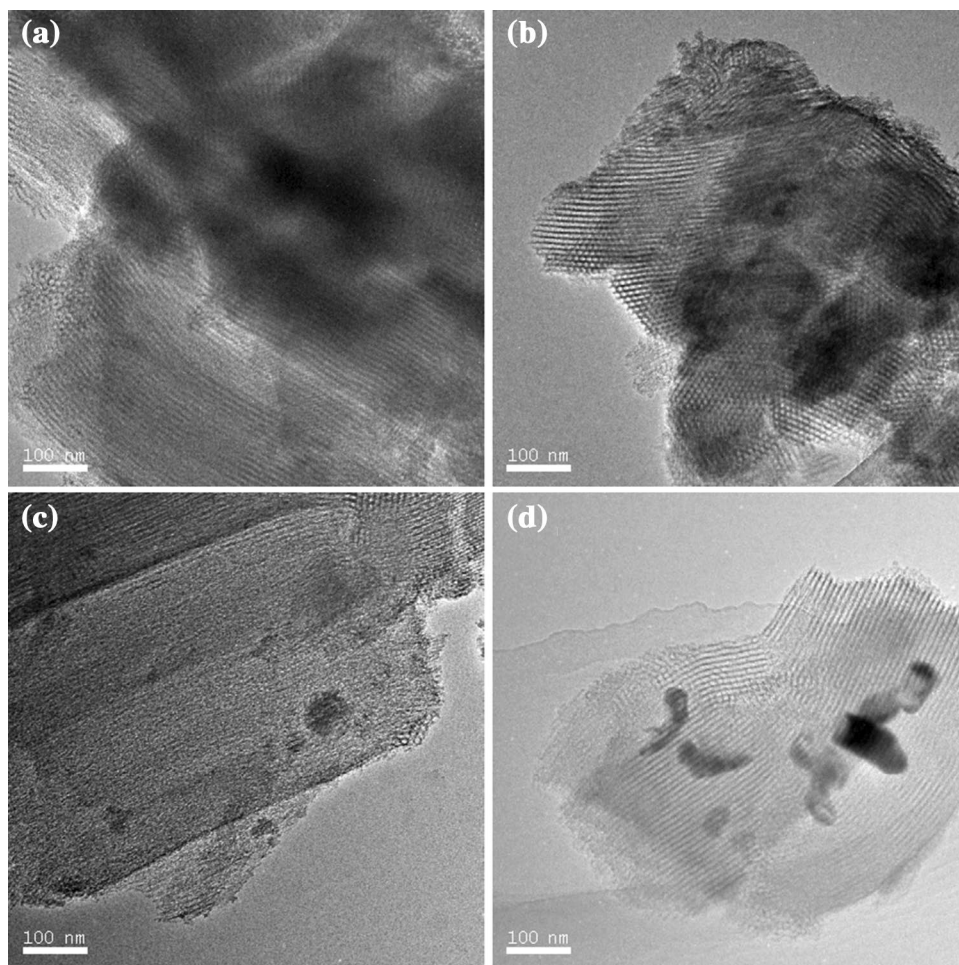
Fig. 4 XRD patterns of **a** calcined and **b** spent Cu/SBA-15 catalysts

Fig. 5 TEM images of the spent catalysts. **a** 1Cu/SBA-15, **b** 2Cu/SBA-15, **c** 3Cu/SBA-15 and **d** 4Cu/SBA-15
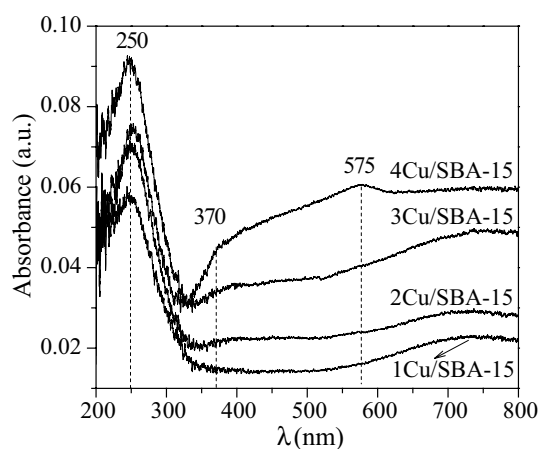
Fig. 6 UV–vis DRS spectra of the spent catalysts

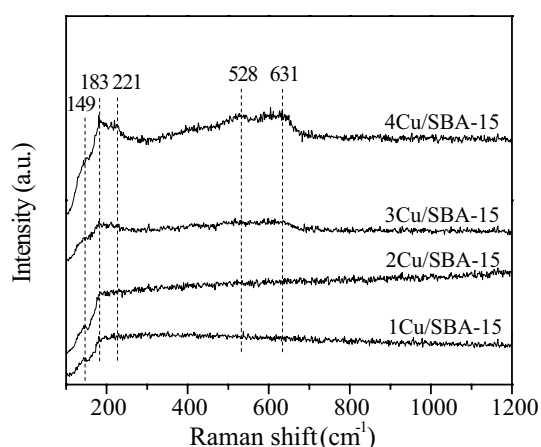**Fig. 8** H$_2$-TPR patterns of Cu/SBA-15 catalysts

Fig. 7 Raman spectra of the spent catalysts

spectra present the similar trend with UV–vis DRS spectra. The signals located at 149, 221, 528 and 631 cm^{-1} are assigned to Cu$_2$O [29–31]. And the 183 cm^{-1} band was also observed in the Raman spectra of chrysocolla [32]. These indicate the existence of well-dispersed Cu species which are small and prone to be oxidized after exposure to air. Nonetheless, the surface species for all catalysts are no difference.

3.2.3 Reduction Properties

The reducibility of all Cu/SBA-15 catalysts was investigated by H$_2$-TPR. Figure 8 displays the reduction plots, and the result of analyses with peak fitting presents in Table 2. Overall, the board H$_2$ consumption band is located in the temperature range of 125–350 °C, which can be assigned to the reduction of Cu^{2+} to Cu^0. The sum of integral area for each catalyst is in well harmony with the concentration of
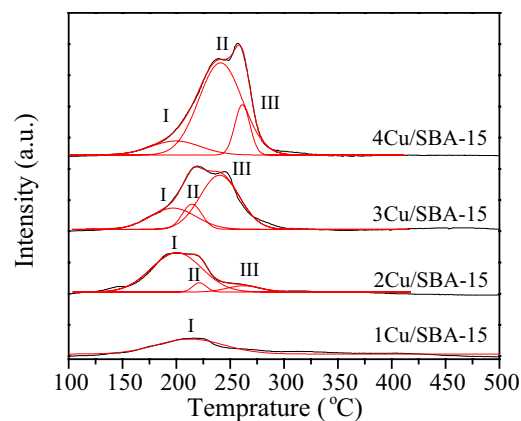
Cu. The correlation is much easier to be viewed by observing the angel between the two variable vectors [33]. And the cosines of the angels were calculated in Table 3. Thus, the H$_2$ evolution rate has better correlation with the area of peak I than that with the sum of area (or Cu content). This indicates that the highly catalytic activity contributed mainly to the smaller and highly dispersed Cu particles. Furthermore, the temperature of reduction peak for 2Cu/SBA-15 is the lowest of all, and the maximum H$_2$ consumption (about two times) in peak I. This explains that more amounts of small Cu particles is existed in the 2Cu/SBA-15, compared with that on the other catalysts [22, 34], and just proves its lowest active energy barrier.

In addition, the formation of large Cu particles for 3Cu/SBA-15 and 4Cu/SBA-15 is not profit for the exposure of active sites, and leads to low hydrogen evolution rate. For the 1Cu/SBA-15 catalyst, a large reduction band was presented, due to the strong interaction with the support [15, 35]. Although small CuO particles on the surface of 1Cu/SBA-15 were formed after calcination, they are more liable to sinter in the reduction process. Thus, a suitable Cu content is needed for amounts of stable and small Cu particles or active sites of cyclohexane dehydrogenation.

3.2.4 Stability Test

The stability test of 2Cu/SBA-15 at 350 °C is shown in Fig. 9. Although the catalyst after operating for 20 h time-on-stream appeared a slight activity loss, the drop in H$_2$ evolution rate tended to vary gently with increasing reaction time. This is attributed to the Cu sintering or carbon formation caused by the high active of small Cu nano-particles. However, these active sites are limited in quantity, and declined at such high temperature and long time-on-stream. Therefore, the amounts of

Table 2 H$_2$-TPR analysis of Cu/SBA-15 catalysts

Catalyst	Area				Center (°C)		
	Peak I	Peak II	Peak III	Sum	Peak I	Peak II	Peak III
1Cu/SBA-15	18,697			18,697	212.8		
2Cu/SBA-15	36,937	2339	3913	43,189	200.3	221.5	262.5
3Cu/SBA-15	18,014	9171	39,812	66,997	196.9	214.5	240.1
4Cu/SBA-15	12,950	74,337	14,149	87,287	199.3	241.0	261.3

Table 3 The cosines of the angel between the two variable vectors

Variable vector[a]	Area$_{Sum}$	Area$_{Peak\ I}$
Cu content	0.9943	–
H$_2$ evolution rate	0.8435	0.9896

[a]The properties of catalysts were represented as a vector. For example, the Cu content was denoted as (1.88, 3.70, 5.45, 7.13)
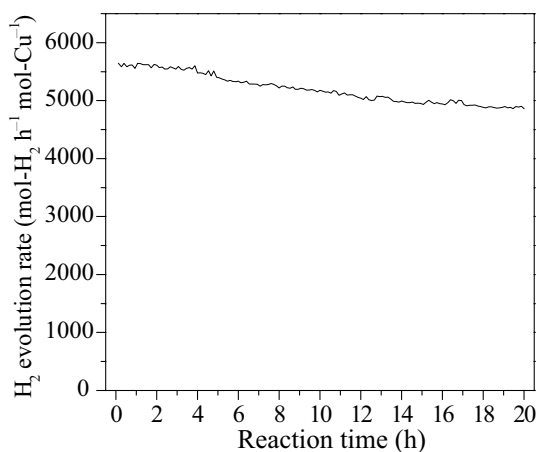
Fig. 9 Stable test of 2Cu/SBA-15 catalyst (150 mg, 350 °C, total 101 kPa, C$_6$H$_{12}$: H$_2$ = 1:25, GHSV = 12,000 h^{-1})

stable Cu particles play a predominant role in maintaining the main dehydrogenation activity.

4 Conclusions

In this work, for high selectivity of cyclohexane dehydrogenation, a series of Cu/SBA-15 catalysts were prepared by impregnation method with different Cu content. They show a 100% selectivity to benzene and the same Cu species on their surface. Moreover, the smaller Cu nanoparticles exhibit higher hydrogen evolution rate or lower active energy barrier. However, they are prone to sinter after reduction, especially to 1Cu/SBA-15 with the lowest Cu content. The 2Cu/SBA-15 was provided with an appropriate Cu content, and lead to form amounts of stable and small Cu particles after high-temperature treatment.

References

1. Schlapbach L, Zuttel A (2001) Nature 414:353–358
2. Alhumaidan F, Cresswell D, Garforth A (2011) Energy Fuels 25:4217–4234
3. Durbin DJ, Malardier-Jugroot C (2013) Int J Hydrog Energy 38:14598–14617
4. Boufaden N, Akkari R, Pawelec B, Fierro JLG, Zina MS, Ghorbel A (2015) Appl Catal A 502:329–339
5. Lee G, Jeong Y, Kim BG, Han JS, Jeong H, Na HB, Jung JC (2015) Catal Commun 67:40–44
6. Pradhan AU, Shukla A, Pande JV, Karmarkar S, Biniwale RB (2011) Int J Hydrog Energy 36:680–688
7. Pande JV, Shukla A, Biniwale RB (2012) Int J Hydrog Energy 37:6756–6763
8. Xia Z, Lu H, Liu H, Zhang Z, Chen Y (2017) Catal Commun 90:39–42
9. Patil SP, Pande JV, Biniwale RB (2013) Int J Hydrog Energy 38:15233–15241
10. Gianotti E, Taillades-Jacquin M, Reyes-Carmona A, Taillades G, Roziere J, Jones DJ (2016) Appl Catal B 185:233–241
11. Wang B, Froment GF, Goodman DW (2008) J Catal 253:239–243
12. Sinfelt JH, Carter JL, Yates DJC (1972) J Catal 24:283–296
13. Ungureanu A, Dragoi B, Chirieac A, Ciotonea C, Royer S, Duprez D, Mamede AS, Dumitriu E (2013) ACS Appl Mater Interfaces 5:3010–3021
14. Vargas-Hernandez D, Rubio-Caballero JM, Santamaria-Gonzalez J, Moreno-Tost R, Merida-Robles JM, Perez-Cruz MA, Jimenez-Lopez A, Hernandez-Huesca R, Maireles-Torres P (2014) J Mol Catal A 383–384:106–113
15. Wang ZQ, Xu ZN, Peng SY, Zhang MJ, Lu G, Chen QS, Chen YC, Guo GC (2015) ACS Catal 5:4255–4259
16. Yin A, Wen C, Guo X, Dai W, Fan K (2011) J Catal 280:77–88
17. Rioux RM, Vannice MA (2003) J Catal 216:362–376
18. Guo Y, Lu G, Mo X, Wang Y (2005) Catal Lett 99:105–108
19. Chen CS, Lai YT, Lai TW, Wu JH, Chen CH, Lee JF, Kao HM (2013) ACS Catal 3:667–677
20. Peppley BA, Amphlett JC, Kearns LM, Mann RF (1999) Appl Catal A 179:21–29
21. Reske R, Mistry H, Behafarid F, Roldan CB, Strasser P (2014) J Am Chem Soc 136:6978–6986
22. Tu CH, Wang AQ, Zheng MY, Wang XD, Zhang T (2006) Appl Catal A 297:40–47
23. Karthikeyan S, Pachamuthu MP, Isaacs MA, Kumar S, Lee AF, Sekaran G (2016) Appl Catal B 199:323–330
24. Chen CS, Chen CC, Chen CT, Kao HM (2011) Chem Commun 47:2288–2290
25. Chen LC, Cheng H, Chiang CW, Lin SD (2015) ChemSusChem 8:1787–1793
26. Feng J, Liu Y, Yin M, He Y, Zhao J, Sun J, Li D (2016) J Catal 344:854–864
27. Marshall CD, Speth JA, Payne SA (1997) J Non-Cryst Solids 212:59–73

28. Pestryakov AN, Petranovskii VP, Kryazhov A, Ozhere-liev O, Pfander N, Knop-Gericke A (2004) Chem Phys Lett 385:173–176
29. Debbichi L, Marco de Lucas MC, Pierson JF, Kruger P (2012) J Phys Chem C 116:10232–10237
30. Jagminas A, Niaura G, Kuzmarskyte J, Butkiene R (2004) Appl Surf Sci 225:302–308
31. Niaura G (2000) Electrochim Acta 45:3507–3519
32. Frost RL, Xi Y (2013) Vib Spectrosc 64:33–38
33. Rodgers JL, Nicewander WA (1988) Am Stat 42:59–66
34. Liu Z, Amiridis MD, Chen Y (2005) J Phys Chem B 109:1251–1255
35. Di W, Cheng J, Tian S, Li J, Chen J, Sun Q (2016) Appl Catal A 510:244–259